Journal of Hydrology 653 (2025) 132746

Contents lists available at ScienceDirect

Journal of Hydrology

journal homepage: www.elsevier.com/locate/jhydrol

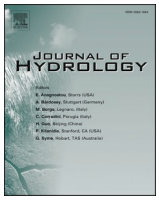

Research papers

Rainfall elasticity functions explain divergent runoff sensitivity to rainfall errors in hydrological models

E. Dallan [a,g,*], T. Perez-Ciria [b], L. Giovannini [c], S. Davolio [d,f], D. Zardi [c,e], M. Borga [a,g]

[a] Department of Land, Environment, Agriculture and Forestry, University of Padova, Padova, Italy
[b] Munich Re, Munich, Germany
[c] Department of Civil, Environmental and Mechanical Engineering (DICAM), University of Trento, Trento, Italy
[d] Dipartimento di Scienze della Terra "A. Desio", Università degli Studi di Milano, 20133 Milan, Italy
[e] Center Agriculture Food Environment (C3A), University of Trento, San Michele all'Adige, Italy
[f] Institute of Atmospheric Sciences and Climate, National Research Council, CNR-ISAC, Bologna, Italy
[g] Research Center on Climate Change Impacts, University of Padova, Rovigo, Italy

ARTICLE INFO

Keywords:
Hydrological modelling
Hydrological model uncertainty
Rainfall error propagation
Elasticity

ABSTRACT

Despite numerous past and ongoing efforts towards characterizing the propagation of rainfall estimation uncertainties in rainfall-runoff hydrologic models, modelers struggle to identify the main features that impact how rainfall errors are transmitted to simulated runoff. With this work, we introduce the concept of the *rainfall elasticity function*, i.e. the measure of how responsive the simulated event runoff is to a change in rainfall. We analytically derive the functions for two well-known runoff generation model types: the Probability Distributed Model (PDM), where the Pareto distribution is used to describe the distribution of soil-moisture storage capacity, and the Soil Conservation Service – Curve Number (SCS-CN) model. These functions are explored to examine the propagation of rainfall errors through the two models. It is shown that the two models are characterized by very different elasticity functions, which results in diverging propagation features of the rainfall errors. For the PDM case, increasing the precipitation depth, or reducing the storage capacity, results in the elasticity growing from 1 to a peak whose value and location depend on the model parameters, and then asymptotically decreases again to 1. For the SCS-CN model, increasing the precipitation depth, or decreasing the maximum potential retention, makes the elasticity decrease from infinity to 1. The capability of the elasticity functions to describe the propagation of rainfall errors through the models is illustrated by using the data from the Vaia 2018 flood in the Eastern Italian Alps. Owing to the very dry initial conditions and the extremely high precipitation depth associated with the event, application to this case allows exploring the whole range of hydrological conditions characterizing the elasticity functions. It is shown that the analytical functions closely resemble the results obtained by forcing the models with the actual distribution of rainfall errors, thus paving the way for the practical application of this approach, such as in hydrological model calibration, and the use of multi-model ensemble for flood forecasting.

1. Introduction

Rainfall is arguably the most important, and yet the most variable input for rainfall-runoff hydrologic models. Indeed, its intrinsic variability and the errors associated with its estimate affect hydrologic simulations in several ways. Despite numerous past and ongoing efforts towards characterizing propagation of rainfall estimation uncertainties in rainfall-runoff hydrologic models, modelers continue to struggle to identify the main features that impact how rainfall errors are transmitted to simulated runoff (e.g. Zoccatelli et al., 2011; Zhu et al., 2013; Ehsan Bhuiyan et al. 2019; Nanding et al., 2021). There is a consensus in the hydrologic community that this issue is still a major challenge from both the theoretical and operational viewpoints.

An extensive review reported by Nanding et al. (2021) shows that a linear relationship is often identified in the literature between precipitation and runoff simulation errors. Due to the strong nonlinearity

* Corresponding author.
E-mail address: eleonora.dallan@unipd.it (E. Dallan).

https://doi.org/10.1016/j.jhydrol.2025.132746
Received 13 June 2024; Received in revised form 20 November 2024; Accepted 12 January 2025
Available online 26 January 2025
0022-1694/© 2025 The Author(s). Published by Elsevier B.V. This is an open access article under the CC BY license (http://creativecommons.org/licenses/by/4.0/).

characterizing most hydrological models, precipitation errors can be either amplified or dampened in simulated discharge in different river basins (Gourley et al. 2011; Nikolopoulos et al. 2013; Beck et al., 2017; Ehsan Bhuiyan et al. 2019; Gou et al., 2024). Moreover, propagation of precipitation errors through hydrological modeling varies with seasons (Biemans et al. 2009) and dampening or amplification of errors depends on rainfall products and basin sizes (Maggioni et al. 2013; Nijssen and Lettenmaier 2004; Nikolopoulos et al. 2010). Nikolopoulos et al. (2010) also report that precipitation error propagation depends on the error metric, indicating that the propagation of rainfall errors into runoff volume results in completely different conclusions than propagation from the same errors into runoff peaks.

This shows that precipitation error propagation through a hydrological model remains unclear and sometimes controversial (Nikolopoulos et al., 2010; Nanding et al., 2021; Ghimire et al., 2022). To the best of our knowledge, the impact of the hydrological model structure on the propagation of precipitation error to runoff simulation has received little attention, except several works showing that infiltration-excess-type models are more sensitive to precipitation inputs than saturation-excess-type models (Winchell et al., 1998; Koren et al., 1999).

The purpose of this paper is to examine how precipitation errors propagate through hydrological models characterized by different structures and how the precipitation amount and the initial soil moisture status impact the propagation. To attain this aim, we focus on the direct runoff generation model and introduce the so-called 'rainfall elasticity function of runoff', characteristic of a specific model structure. The rainfall elasticity function quantifies the variation of simulated runoff to a change in rainfall by analytical derivation. The analytical derivation allows one to isolate the direct impact of key variables like rainfall depth and initial soil moisture status, with a clear interpretation of the results.

In this work, we analytically derive the rainfall elasticity function for two well-known runoff generation model types: the Probability Distributed Model (PDM) (Moore, 1985, 2007), where the Pareto distribution is used to describe the distribution of soil moisture storage capacity, and the SCS-CN model (Mockus, 1972). These two runoff-generation models are integrated into several hydrological models. For instance, the probability distributed principle is included in the Xinanjiang model (Zhao et al., 1992), the variable infiltration capacity (VIC) model (Liang et al., 1994) and the Arno model (Todini, 1996). The SCS-CN model has been integrated into several rainfall-runoff models, as shown by Singh and Frevert (2002), where at least 6 of the 22 chapters present mathematical models of watershed hydrology that use the SCS-CN approach. Examining these two models is thus highly relevant. Besides being of widespread use, the two models rely on one main common assumption, as their direct runoff depth simulation is time-independent, i.e. the computation of the runoff depth depends only on rainfall depth and is independent of the time distribution of the rainfall input.

The main differences between the elasticity functions of the two models and the relevant implications are analyzed in detail. An application to a major flood event in the Eastern Italian Alps, where the two hydrological models were forced with a Numerical Weather Prediction (NWP) model, permits to examine the capability of the elasticity functions to isolate the main characteristics of the rainfall error propagation. Implications of these findings for runoff model calibration and the use of hydrological models in flood forecasting are discussed in the Conclusion section.

2. The rainfall elasticity function

Elasticity is a measure of how sensitive a variable, in our case runoff, is to a change in another variable, such as rainfall, quantified as the ratio of the percentage change in one variable to the percentage change in the other variable (Schaake, 1990). Although annual elasticity is usually considered in the literature (Andreassian et al., 2016; Hunt et al., 2023 Anderson et al., 2024), here we extend the concept to the representation of the rainfall elasticity function of runoff depth of a flood event, by exploiting the usual definition of elasticity (Schaake, 1990):

$$\frac{\Delta Q}{Q} = \varepsilon(P, Q, modelparameters)\frac{\Delta P}{P} \tag{1}$$

and hence

$$\varepsilon = \frac{P}{Q}\frac{\Delta Q}{\Delta P} \tag{2}$$

where Q is the flood event runoff, P denotes the net driving rainfall input (assumed to be spatially uniform) and ε represents the elasticity function. This expression of rainfall elasticity is coherent with the one used for the scope of sensitivity analysis in Loucks and van Beek (2005). For several applications of hydrological models under flood conditions, the dominant model controlling the elasticity function is the direct runoff routine (Markstrom et al., 2016) and the structure of the corresponding runoff generation model permits an analytical representation of the elasticity function, as follows:

$$\boldsymbol{\varepsilon} = \frac{\boldsymbol{P}}{\boldsymbol{Q}}\frac{\partial \boldsymbol{Q}}{\partial \boldsymbol{P}} \tag{3}$$

An analytical representation of the rainfall elasticity function provides a convenient illustration of the main controlling variables of the rainfall elasticity. It more specifically allows one to analyze the relationship between rainfall elasticity and the rainfall depth itself, as well as its dependence on different initial soil moisture conditions. This is key information, as it allows one to identify the conditions that, for instance, maximize the sensitivity of runoff simulation to rainfall estimation errors. It should be mentioned that the identification of the rainfall elasticity function relies on one main assumption, i.e. the computation of the runoff depth depends only on rainfall depth and is independent of the time distribution of the rainfall input.

The analytical derivation of the rainfall elasticity function is carried out in the following sections for the Probability Distributed Model (PDM), where the Pareto distribution is used to describe the distribution of soil moisture storage capacity, and for the SCS-CN model.

2.1. The probability Distributed model and its elasticity function

In the PDM, runoff production is represented by a saturation-excess runoff process controlled by the absorption capacity of the canopy, surface and soil. The spatial variability of the absorption capacity is described by a probability density function. Here, we consider the generalized Pareto distribution:

$$F(C) = 1 - \left(1 - \frac{C}{C_{max}}\right)^{b} \tag{4}$$

where *F(C)* is the cumulative probability, i.e., the fraction of the catchment area for which the storage capacity is less than *C* (mm), and C_{max} (mm) is the maximum value of the point scale storage capacity over the catchment. The water storage capacity includes vegetation interception, surface retention, and soil moisture capacity. The exponent *b* is the shape parameter of the storage capacity distribution, and controls the degree of spatial variability of storage capacity over the basin. The parameter *b* ranges from 0.01 to 5.0, as suggested by Wood et al. (1992). The storage capacity distribution curve is convex (i.e., the second derivative with *C* is positive) for $0 < b < 1$ and concave (i.e., the second derivative with *C* is negative) for $b > 1$. As reported in Fig. 4 in Moore (1985), in the first case the probability density function describes higher frequency of higher storage capacity values, while, in the second case, a higher frequency of lower storage capacity values. A rectangular distribution is obtained for $b = 1$, whereas $b = 0$ implies a constant storage capacity over the basin (Moore, 2007).

Integrating the exceedance probability of storage capacity provides

the average value over the catchment:

$$C_{med} = \frac{C_{max}}{b+1} \tag{5}$$

The runoff generated during a wet interval, with constant net rainfall (P), is given by the following equations:

$$Q = P - \frac{C_{max}}{b+1}\left[\left(1-\frac{C_o}{C_{max}}\right)^{b+1} - \left(1-\frac{C}{C_{max}}\right)^{b+1}\right] \quad P \le c_{max} - C_o \tag{6}$$

$$Q = P - \frac{C_{max}}{b+1}\left\{1 - \left[1-\left(1-\frac{C_o}{C_{max}}\right)^{b+1}\right]\right\} \quad P > c_{max} - C_o \tag{7}$$

where C_o is the initial storage content. When introducing the normalized rainfall $w_{pdm} = \frac{P}{C_{max}-C_o}$ and the relative initial available capacity $C_i = \frac{C_{max}-C_o}{C_{max}}$, Eqs (6) and (7) read as follows:

$$Q = w_{pdm}C_iC_{max} - \frac{C_{max}}{b+1}\left[(C_i)^{b+1} - \left(1-\frac{C}{C_{max}}\right)^{b+1}\right] \quad w_{pdm} \le 1 \tag{8}$$

$$Q = w_{pdm}C_iC_{max} - \frac{C_{max}}{b+1}\left\{1 - \left[1-(C_i)^{b+1}\right]\right\} \quad w_{pdm} > 1 \tag{9}$$

The first derivative $\alpha_{pdm} = \frac{\partial Q}{\partial P}$ can therefore be expressed as a function of the normalized rainfall w_{pdm} as follows:

$$\alpha_{pdm} = \frac{\partial Q}{\partial P} = 1 - (C_i)^b\left(1-w_{pdm}\right)^b \quad w_{pdm} \le 1 \tag{10}$$

$$\alpha_{pdm} = \frac{\partial Q}{\partial P} = 1 \quad w_{pdm} > 1 \tag{11}$$

The derivative α_{pdm} is shown in Fig. 1 as a function of w_{pdm}, for 5 different values of the relative initial available capacity C_i and three values of the parameter b, representing three different shapes of the storage capacity distribution, as reported above. The figure shows that the derivative α_{pdm} increases to 1 for$w_{pdm} = 1$, and then remains constant and equal to 1 for any larger value of w_{pdm}. This shows that the runoff error is less than the driving rainfall error until the storage capacity is reached. When the storage capacity is exceeded, the runoff error equates to the rainfall error, since all rainfall is transformed into runoff.

The elasticity function ε_{pdm} is then derived from the above equations as follows:

$$\varepsilon_{pdm} = \frac{w_{pdm}\left[1-(C_i)^b\left(1-w_{pdm}\right)^b\right]}{w_{pdm} - (C_i)^b\left[\frac{1-\left(1-w_{pdm}\right)^{b+1}}{b+1}\right]} \quad w_{pdm} \le 1 \tag{12}$$

$$\varepsilon_{pdm} = \frac{w_{pdm}(C_i)}{w_{pdm}(C_i) - \left(\frac{1}{b+1}\right)\left(1-(1-(C_i)^{b+1})\right)} \quad w_{pdm} > 1 \tag{13}$$

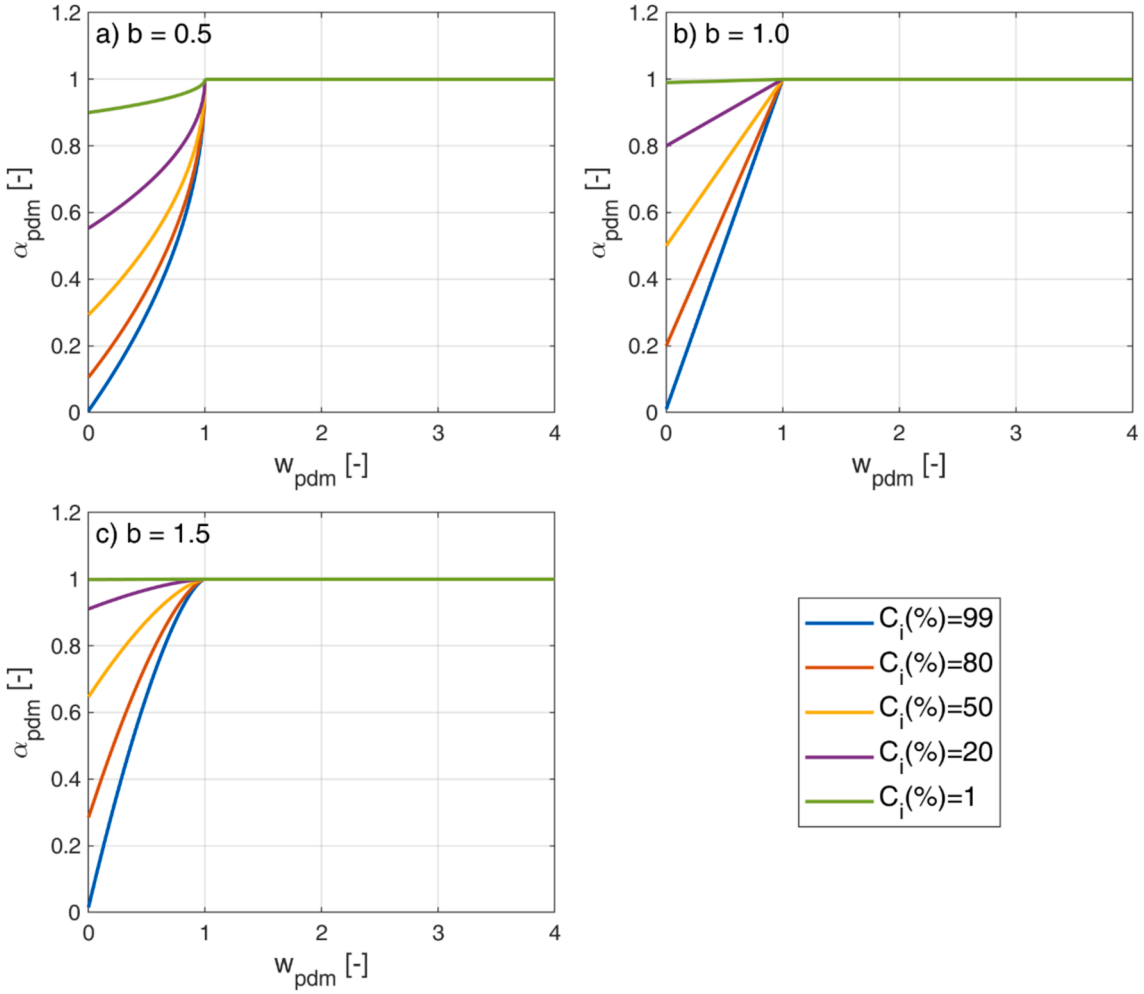

Fig. 1. The α_{pdm} function for the PDM for 5 different values of the relative initial available storage capacity C_i and three values of the parameter b: a) 0.5, b) 1.0, and c) 1.5.

Fig. 2 reports the elasticity function ε_{pdm} as a function of w_{pdm}, for five different values of the relative initial available capacity C_i and three different values of the parameter b.

As is evident from Equations (12) and (13), and Fig. 2, the structure of ε_{pdm} is strongly linked to that of α_{pdm}. The elasticity is always larger than or equal to 1, implying that the relative runoff error is always larger than (or equal to) the relative rainfall error. For $b \leq 1$, the function shows a peak value $\varepsilon_{pdm,max}$ for$w_{pdm} = 1$, implying that the sensitivity of runoff relative error to relative rainfall error peaks with rainfall depths corresponding to the model soil moisture capacity. For $b > 1$, the elasticity peak shifts towards$w_{pdm} = 0$, with peak values not higher than 2. The elasticity peak $\varepsilon_{pdm,max}$ varies, irrespective of the parameter b, with the relative initial available capacity C_i, with higher $\varepsilon_{pdm,max}$ with increasing C_i. This implies that the sensitivity of runoff relative error to relative rainfall error is larger with drier initial conditions (low runoff generation). Conversely, the degree of sensitivity is at a minimum, i.e. close to 1, under wet initial conditions.

The variation of the value of ε_{pdm} for$w_{pdm} = 1$, termed here $\varepsilon_{pdm,w=1}$, with the variation of the PDM parameters C_i and b is reported in Fig. 3. For $b \leq 1$, the value represents the peak of the function and, as such, its features are of particular interest. The figure shows that $\varepsilon_{pdm,w=1}$ increases quickly with reducing the value of b and increasing the value of C_i. For $b \leq 0.2$ and $C_i \geq 0.5$, the value of $\varepsilon_{pdm,w=1}$ may exceed 5. For reduced b and increased C_i, the initial storage capacity is higher, thus describing drier initial conditions and lower runoff generation.

Practical applications of the elasticity concepts in runoff modeling entail discrete values of ΔP, which may represent rainfall estimation/forecasting errors, instead of an infinitesimally small increment dP. The effects of using discrete values of ΔP on the elasticity function are captured by reporting the values of $\frac{P}{Q}\frac{\Delta Q}{\Delta P}$, for values of ΔP corresponding to two multiplicative errors on P, namely + 0.2P and −0.2P, for $C_i = 0.5$ and the three values of b (Fig. 4).

The figure shows that the changes in elasticity are not symmetric with respect to under- or overestimation errors. In particular, elasticity is attenuated in case of rainfall underestimation (−0.2P), and this effect is particularly remarkable for $b \leq 1$, as expected given that the peak is particularly sharp in that range of values. The peak shifts toward values of $w_{pdm} > 1$, and the attenuation effect on elasticity disappears after reaching the peak. On the other hand, in the case of overestimation of P (+0.2P), the elasticity is enhanced, and its peak moves to $w_{pdm} < 1$.

2.2. The SCS-CN model and its elasticity function

The general SCS-CN runoff equation is as follows:

$$Q = \frac{(P - I_a)^2}{P - I_a + S} \quad P \geq I_a \qquad Q = 0 \quad P \geq I_a \tag{14}$$

where I_a, the so called 'initial abstraction', represents an amount of rainfall that is retained in the watershed storage by interception, infiltration, and surface storage before the runoff begins (Ponce and Hawkins, 1996), and S is a site storage index defined as maximum potential retention. By convention, the initial abstraction is a fraction of the maximum potential retention, i.e. $I_a = \gamma S$, where γ is the initial

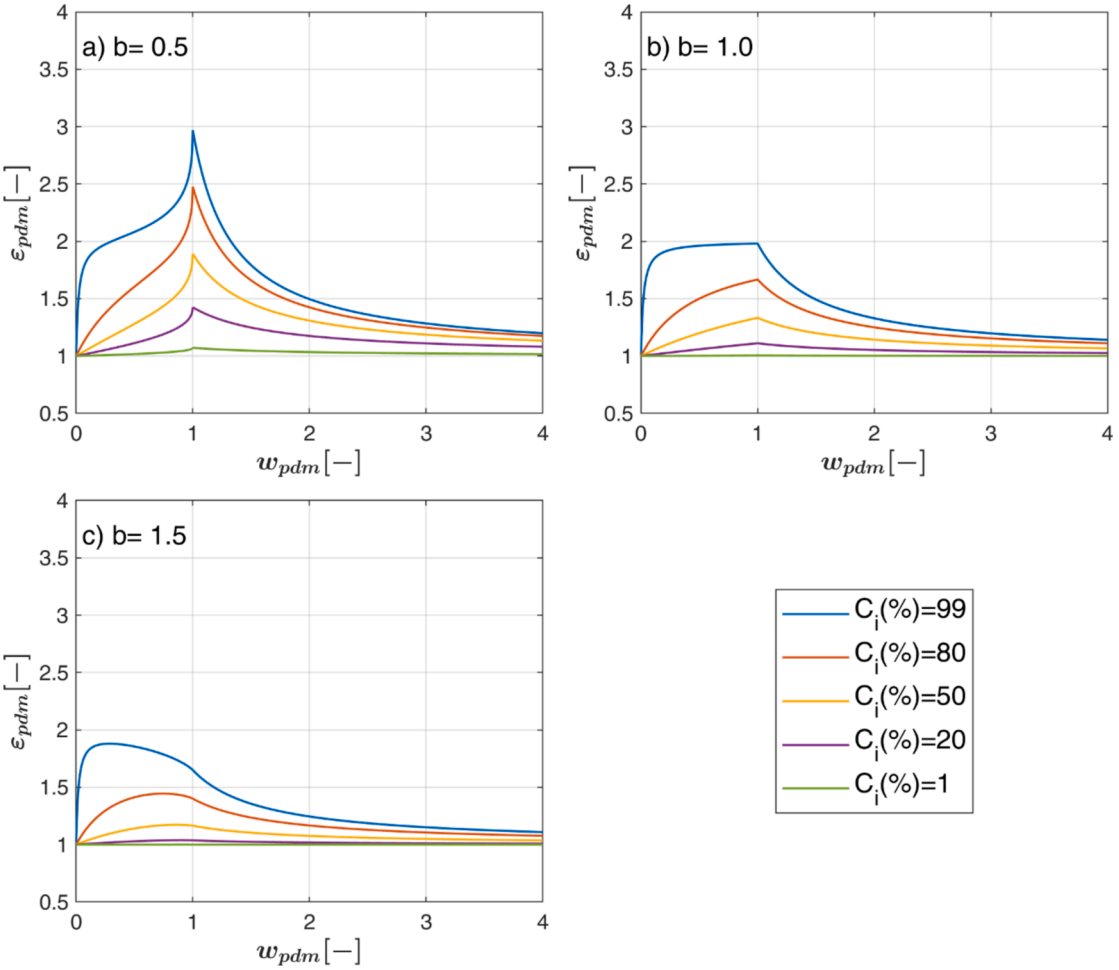

Fig. 2. The elasticity function ε_{pdm} for five different values of relative initial available capacity C_i and three values of the parameter b: a) 0.5, b) 1.0, and c) 1.5.

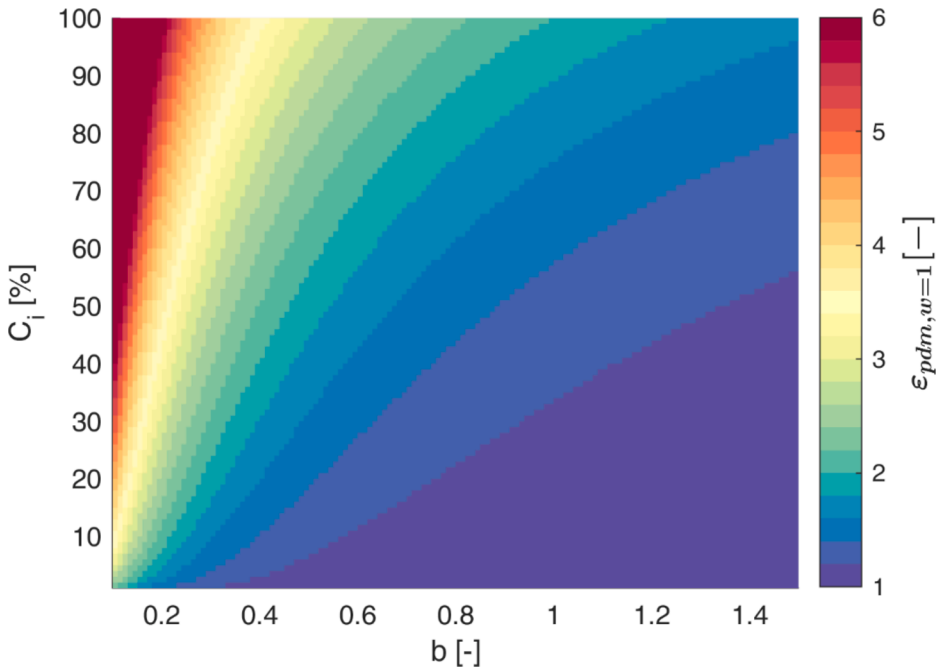

Fig. 3. Variation of the value of $\varepsilon_{pdm,w=1}$ as a function of the PDM model parameters b and C_i.

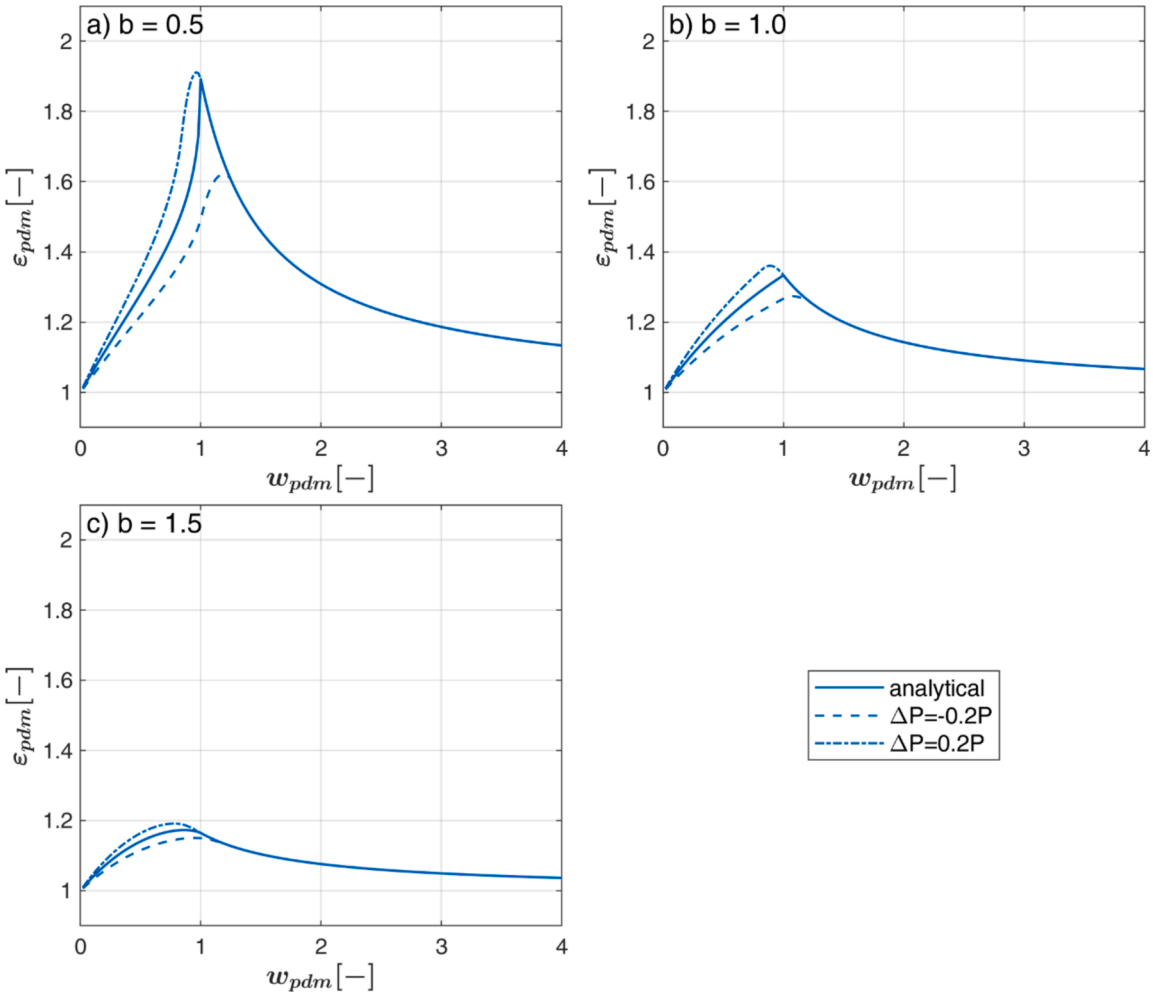

Fig. 4. Effect of using discrete values of ΔP on the elasticity function, for two values of ΔP corresponding to + 0.2P and −0.2P, for $C_i = 0.5$ and three values of the parameter b: a) 0.5, b) 1.0, and c) 1.5.

abstraction ratio. The standard value for the parameter γ is 0.2, but a value of 0.05 is usually considered to be more realistic (Ponce and Hawkins, 1996). All variables in Eq. (14) have length units, and the equation is dimensionally homogeneous. The maximum potential retention S is defined by the dimensionless CN parameter, as follows:

$$CN = 254\left(\frac{100}{254+S}\right) \tag{15}$$

CN, which may take values from 0 to 100, is a function of the hydrological soil type, land use and treatment, ground surface conditions and antecedent soil moisture conditions. Eq. (14) allows computing the runoff response for a rainfall event. The incremental excess for a time interval is computed as the difference between the accumulated excess at the end and at the beginning of the period.

The first derivative of Eq. (14) with respect to P is as follows:

$$\frac{\partial Q}{\partial P} = \alpha_{CN} = 1 - \left[\frac{1}{(w_{CN}+1)(1-\gamma)}\right]^2 \qquad w_{CN} \geq \frac{\gamma}{1-\gamma} \tag{16}$$

where $w_{CN} = \frac{P}{S(1-\gamma)}$, under the constraint $w_{CN} \geq \frac{\gamma}{1-\gamma}$. Fig. 5 reports the values α_{CN} as a function of w_{CN}, showing that as w_{CN} tends to $\frac{\gamma}{1-\gamma}$, α_{CN} tends to 0, and as w_{CN} tends to ∞, then α_{CN} tends to 1. Analogously to the PDM case, this means that the runoff error is always less than the driving rainfall error, as part of this error is propagated into the soil moisture. However, in this case the function never reaches the unitary value. The vertical dashed lines in Fig. 5 define the domain of validity for the α_{CN} function, represented by the condition $w_{CN} \geq \frac{\gamma}{1-\gamma}$.

The rainfall elasticity function can be written as follows:

$$\varepsilon_{CN} = \frac{w_{CN}[w_{CN}(1-\gamma)-\gamma+2]}{[w_{CN}+1][w_{CN}(1-\gamma)-\gamma]} \qquad w_{CN} \geq \frac{\gamma}{1-\gamma} \tag{17}$$

Fig. 6 shows that the elasticity ε_{CN} is always larger than 1. It is evident from Eq. (17) that ε_{CN} tends to ∞ as w_{CN} tends to $\frac{\gamma}{1-\gamma}$ whereas ε_{CN} tends to 1 as w_{CN} tends to ∞. This means that the relative runoff error is always larger than the relative rainfall error, as for the PDM model. Furthermore, for any value of S, the sensitivity is larger for values of P close to I_a, whereas it is close to 1 for large values of P. Conversely, given a value of P, the elasticity is larger for values of I_a close to P and it is close to 1 for small values of S.

These results suggest that the antecedent moisture conditions have a remarkable effect on the sensitivity of the model to relative rainfall errors, with dry antecedent conditions leading to higher sensitivity to rainfall errors than wet conditions. In general, conditions that increase

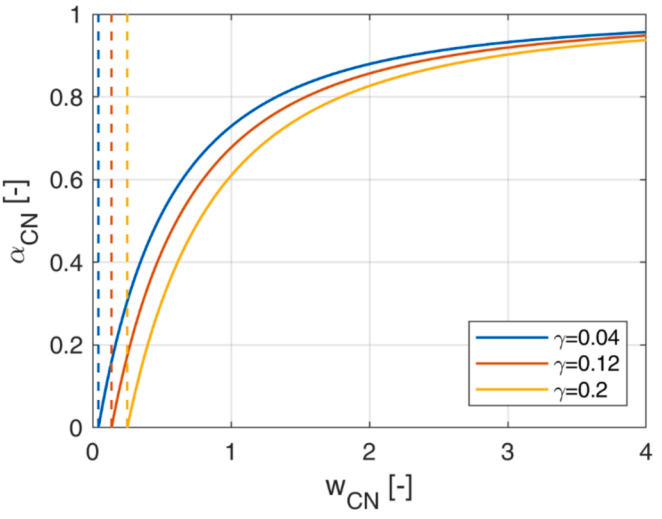

Fig. 5. The α_{CN} function for the SCS-CN model for $\gamma = 0.04$, 0.12 and 0.2; the vertical dashed lines indicate the domain of validity $w_{CN} \geq \frac{\gamma}{1-\gamma}$.

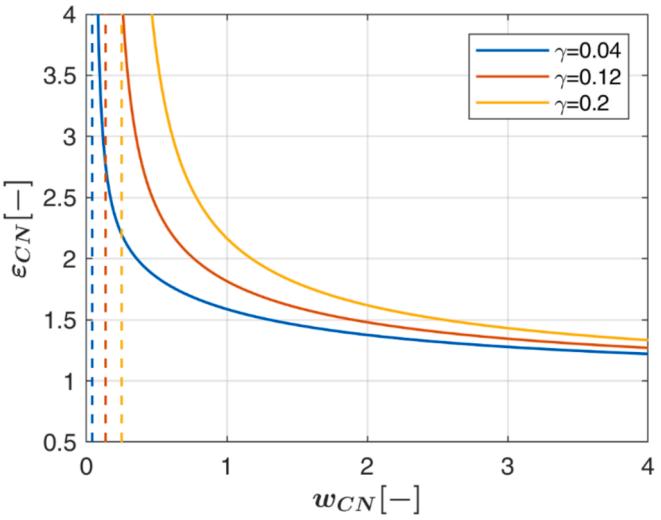

Fig. 6. The elasticity function ε_{CN} for $\gamma = 0.04$, 0.12 and 0.2. The vertical dashed lines indicate the domain of validity $w_{CN} \geq \frac{\gamma}{1-\gamma}$.

the percentage of infiltration losses (such as dry initial conditions and small storms just above the runoff-initiation threshold) lead to higher runoff sensitivity to rainfall errors. Conversely, the degree of sensitivity is minimal (i.e. close to 1) for conditions typically conducive to severe flooding: wet initial conditions and large rainfall depths.

Analogously to the PDM case, the effects of using discrete values of ΔP on the elasticity function are explored by reporting (Fig. 7) the values of $\frac{P}{Q}\frac{\Delta Q}{\Delta P}$ for values of ΔP corresponding to two multiplicative errors on P, +0.2P and −0.2P, for the two limiting cases of $\gamma = 0.04$, and $\gamma = 0.2$.

The figure shows that elasticity is attenuated (enhanced) in case of rainfall underestimation (overestimation), and that the attenuation (enhancement) decreases with increasing w_{CN} (higher value of normalized precipitation, higher runoff generation, lower sensitivity of runoff error to rainfall errors).

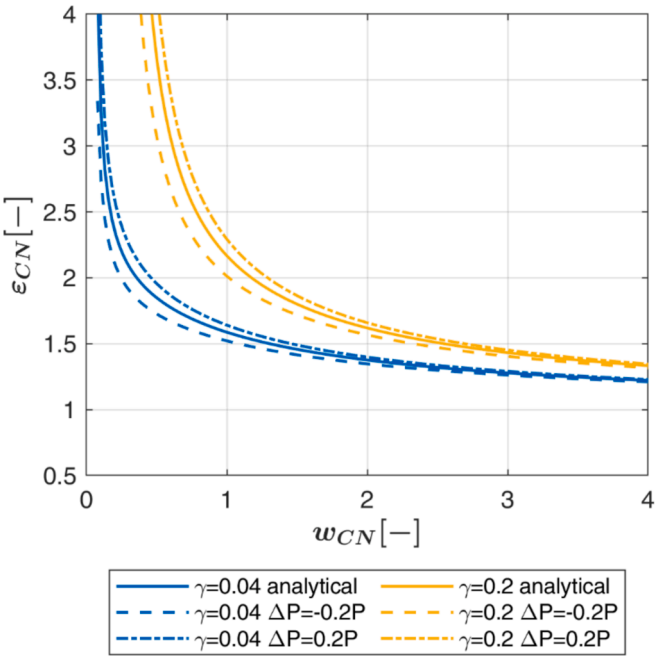

Fig. 7. Effects of using discrete values of ΔP on the elasticity function, for two values of ΔP corresponding to + 0.2P and −0.2P, and for the two limiting cases of $\gamma = 0.04$ and $\gamma = 0.2$.

3. Assessment of the elasticity functions for an extreme flood event

The application of the above-derived elasticity functions for understanding the propagation of rainfall error through hydrological models relies on multiple assumptions, the most important being: i) the use of the analytical elasticity functions closely resembles the elasticity values obtained by considering the actual distribution of rainfall relative errors; ii) the propagation of the rainfall error is mainly impacted by the characteristics of the direct runoff routine, whereas the other conceptual storages, devoted to groundwater simulation and runoff propagation, exert limited influence on the error propagation.

These assumptions are assessed in this Section by using hydrological models that incorporate the two above-described runoff generation models to predict flood response for the Vaia storm (Giovannini et al., 2021), which impacted the Eastern Italian Alps on October 27–29 2018. The study area includes the upper Adige river basin closed at Bronzolo, in the Eastern Italian Alps (Fig. 8), and its internal nested 31 sub-basins. This is an Alpine catchment with a drainage area of 6834 km^2. The nested basins range in drainage area from 20 km^2 to 6834 km^2, with a median value of 156 km^2. The elevation ranges from about 200 m a.s.l. at the southern valley bottoms, to around 3900 m a.s.l. in the western upper ranges, with a mean elevation of around 1800 m a.s.l. The steep terrain and the high elevation gradients control the spatial precipitation distribution, with the mean annual precipitation ranging from 500 mm in the northwestern part to 1600 mm in the southern part (Formetta et al., 2024; Dallan et al., 2022, 2023, 2024a,b).

The Vaia storm occurred at the end of a climatically anomalous prolonged drought. The synoptic situation was characterized by a trough, which deepened over the western Mediterranean basin, developing a wide cyclonic area at the surface while slowly evolving eastward towards northwestern Italy. The storm dropped large precipitation amounts ranging from 150 to 250 mm over the upper Adige River basin. The total precipitation was the highest ever recorded in the area for a flood event lasting 3 days, with a rainstorm severity exceeding 200 years return time for the accumulated precipitation (Giovannini et al., 2021).

The Vaia flood provides an excellent benchmark for testing the elasticity functions. Being characterized by very dry initial conditions followed by extremely high precipitation depth, it permits the exploration of the whole range of hydrological conditions which characterize the elasticity functions. Moreover, thanks to its large spatial extent, it allows comprehensive testing over a relatively large number of different basins.

3.1. Hydrological and NWP models

The conceptual, semi-distributed hydrological model ICHYMOD (Norbiato et al., 2009; 2008; Di Marco et al., 2021) was used to simulate flood responses at hourly time resolution. Two alternative direct runoff generation models were included in ICHYMOD: i) the PDM soil moisture accounting model, with the Pareto probability distribution; and ii) the SCS-CN model. In both cases, the runoff generation models take up water from rainfall and snowmelt. Whereas the PDM soil moisture storage loses water by recharge to the groundwater storage, in the case of the SCS-CN the infiltrated rate computed by the model represents the input to the non-linear groundwater storage (Destro et al., 2018). Direct runoff is routed to the outlet of the sub-basin using a cascade of two linear reservoirs, while baseflow is transferred downstream through the adoption of a nonlinear storage. The well-known Muskingum-Cunge scheme is used to propagate the flow from each sub-basin outlet along the river network. In the following, the complete hydrological model chains, inclusive of the runoff generation models, are termed 'complete hydrological models', whereas the runoff generation models considered in isolation, i.e. represented without taking into account the flows due to evapotranspiration and recharge, are termed 'runoff modules'.

Data from various sources – including two weather radars, a dense network of 120 rain gauge stations and 31 stream gauge stations – are used to implement the two complete hydrological models over the study areas. The two versions of the ICHYMOD model were calibrated over the river system considering a set of flood events not including the Vaia flood (see Norbiato et al., 2008, 2009; Destro et al., 2018; Scorpio et al., 2022). Data from the rain gauges and the two weather radars were merged and provided the precipitation input (hereafter called 'reference' precipitation) to ICHYMOD. The application of ICHYMOD to simulate the Vaia flood event was relatively successful, as confirmed by Nash-Sutcliffe efficiency values (Nash and Sutcliffe, 1970) ranging from 0.58 to 0.85, with the two model implementations providing comparable and overlapping predictions (Dallan et al., in prep.).

Moreover, precipitation hindcasts were obtained for the event with the convection-permitting BOLAM-MOLOCH modeling chain (Davolio

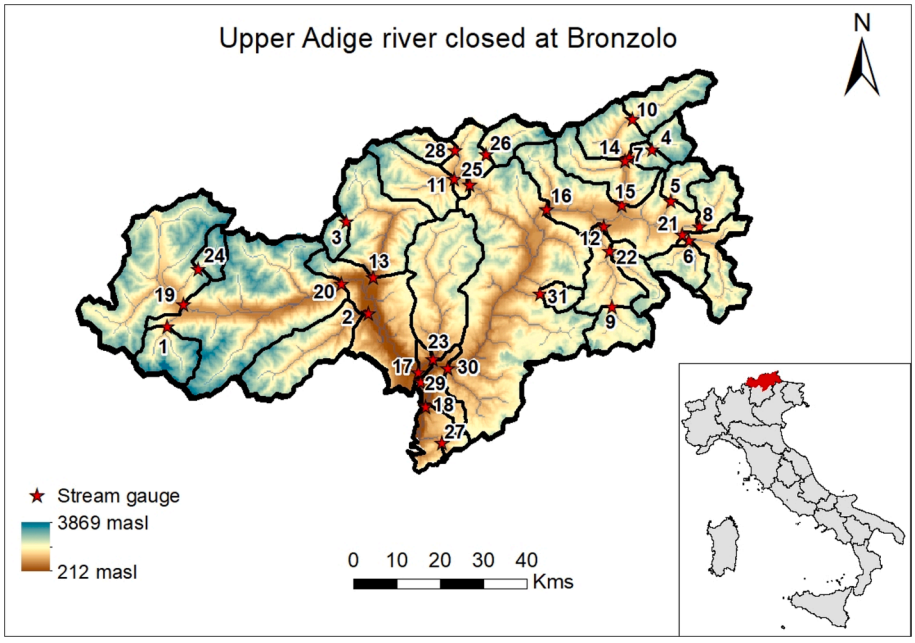

Fig. 8. Study catchments and their location in Italy.

et al., 2020), developed at the Institute of Atmospheric Sciences and Climate of the Italian National Research Council (CNR-ISAC). The final MOLOCH model output is characterized by high spatial (about 1 km) and temporal (1 h) resolution. Simulations covered 96 h, from 00 UTC 26 October 2018 to 00 UTC 30 October 2018. The first 24 h were considered as spin-up time. The initial and boundary conditions for the modeling chain were supplied by the 6-hourly Integrated Forecasting System (IFS) analysis fields on a 0.1-degree grid from the European Center for Medium-Range Weather Forecasts (ECMWF).

The real distribution of the event-accumulated relative rainfall errors is obtained by comparing MOLOCH-derived and reference precipitation. The transmission of these rainfall errors to relative runoff error for the two calibrated models is first quantified using the analytical elasticity functions. These predictions are then compared with those obtained by running the complete hydrological models separately with the reference and MOLOCH-based precipitation inputs. This simulation-based derivation of elasticity values is carried out in two different ways, in order to shed light on the two assumptions listed above. First, elasticity values are obtained based on the two direct runoff modules, to test the impact of using the real distribution of the rainfall errors. Second, elasticity values are derived from runoff simulations obtained by the application of the complete hydrological models, to test the additional impact exerted by the propagation of the errors through the conceptual storages devoted to groundwater simulation and runoff propagation.

In a subsequent evaluation, the direct runoff values obtained from the two runoff modules (PDM and SCS-CN) at each consecutive hour of simulation are exploited to compute a set of elasticity values over the whole flood simulation and the 31 sub-basins. The elasticity values thus obtained are binned over equally-populated classes of normalized rainfall w_{PDM} and w_{CN}. The elasticity value statistics are compared with those obtained from the analytical functions, contrasting corresponding classes. This allows a finer evaluation of the ability of the elasticity functions to describe the propagation of relative rainfall errors with varying normalized precipitation.

3.2. Results

The calibration of the two complete hydrological models leads to identifying of the key PDM and SCS-CN parameters over the 31 study basins. For the PDM case, C_{max} ranges between 310 and 500 mm, whereas the parameter b ranges between 0.13 and 0.6. For the SCS-CN case, CN ranges between 30 and 38, whereas γ ranges between 0.04 and 0.07 (Dallan et al., in prep).

The comparison of the MOLOCH precipitation with the reference precipitation at the basin scale was characterized by very good performances. The relative mean error over the 31 basins amounts to 0.08, whereas the coefficient of determination r^2 equals 0.82 and Nash-Sutcliffe amounts to 0.79. Relative errors range between −0.28 and 0.34.

The statistical features of the elasticity values obtained by running the models and computed through the analytical elasticity functions are reported in Fig. 9, for the two runoff generation modules and the two complete hydrological models. As expected, there important differences exist between the PDM and the SCS-CN runoff generation models. With the very high precipitation depths roughly close to 75 % of C_{max} and to 0.5 S_{max}, and for the range of considered model parameters, the value of the analytically derived elasticity is expected to be between 1.5 and 2 for the PDM, and larger than 2 for the SCS-CN model. This is reflected in the results, which show that the PDM analytical elasticity ranges between 1.35 and 2.1, with a median equal to 1.79, whereas the SCS-CN analytical elasticity ranges between 1.65 and 2.31, with a median equal to 2.07. This shows that the SCS-CN is generally more sensitive to rainfall errors for this event, with an increase of 28 % with respect to the PDM, when the comparison is carried out among the medians.

The use of the distribution of rainfall errors associated with the NWP models with the two runoff-generation modules leads to inflated ranges of elasticity, in agreement with the results reported in Fig. 4 and Fig. 7. The PDM elasticity ranges between 1.19 and 2.21, with a median equal to 1.75, whereas the SCS-CN elasticity ranges between 1.53 and 2.75, with a median equal to 2.05. Even though the ranges increase, the median value remains close to the one computed byusing analytical derivation, supporting the robustness of the results obtained by using the analytical functions.

The question concerning the transmission of the rainfall errors through the complete chain of the two hydrological models is the main question for practical and operational purposes. In this case, the runoff relative errors are propagated not only through the direct runoff routines, but also through the groundwater storage and propagation modules. The elasticity values are modified in a model-dependent way. The PDM elasticity ranges between 1.09 and 1.91, with a median equal to 1.65, showing a general reduction of the elasticity distribution. Conversely, the SCS-CN elasticity ranges between 1.5 and 2.74, with a median equal to 2.06, implying an invariance of the elasticity values with respect to those computed in the previous step. Only for the PDM case, the error propagation through the complete model shows a remarkable difference with respect to the case of runoff generation. Indeed, the content of the PDM storage is depleted by the drainage to the subsurface storage and by evapotranspiration, an aspect that is not accounted for in the analytical case and when the rainfall errors are propagated through the direct runoff routine. This leads to a reduction

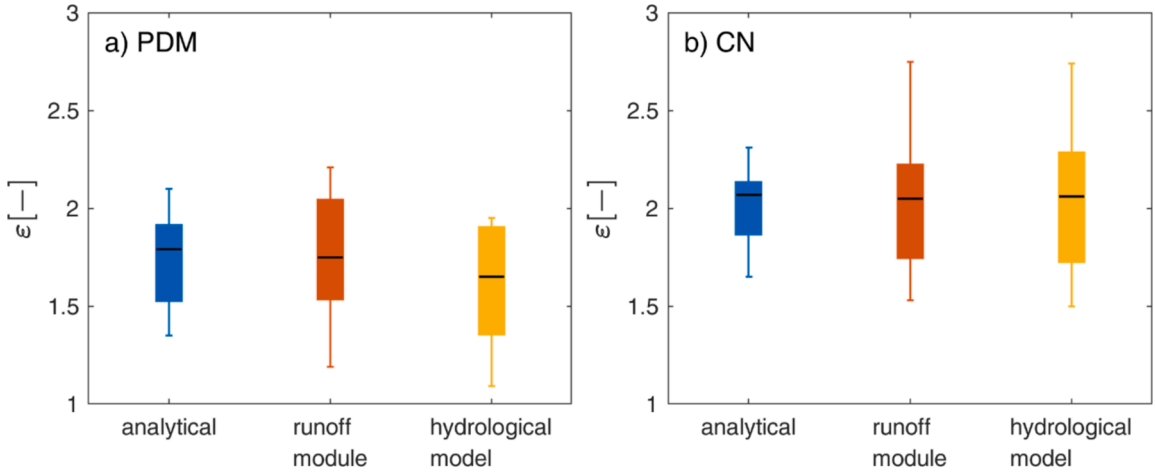

Fig. 9. Elasticity values obtained by using the analytically-derived elasticity functions (*analytical function*), the runoff generation module (*runoff module*), and the complete chain of hydrological models (*hydrological model*), for a) PDM, and b) SCS-CN modules.

of the elasticity values, as shown in Fig. 9a. Conversely, this does not occur in the SCS-CN case, where the input to the groundwater storage is provided directly by the infiltrated water.

The close resemblance between the elasticity values obtained by the use of the whole hydrological model and those obtained from running the NWP rainfall errors through the two direct runoff routines implies that the latter can be used as a reference to evaluate the quality of the analytically derived elasticity values along the whole flood simulation at hourly time step (Fig. 10). The figure shows that the analytically derived elasticity values compare very well with those obtained from the distribution of NWP rainfall errors with the runoff modules (i.e., without considering the flows due to evapotranspiration and to recharge), thus confirming the capability of the analytical framework to reproduce the elasticity across a wide range of normalized precipitation values.

4. Discussion

The results presented in this paper clearly demonstrate that the magnitude and dynamics of precipitation-related errors in direct runoff simulations depend not only on the uncertainty of precipitation but also on the structure of the direct runoff module applied for the hydrologic simulation. Examining of the dependence of the two elasticity functions on the normalized precipitation in Fig. 2 and Fig. 6 shows important analogies. The elasticity is always larger than 1, and it tends to 1 for normalized precipitation values approaching infinity. For both the models, the elasticity is higher when initial conditions are drier (described by a higher initial storage capacity C_i for PDM and a higher parameter γ for the SCS-CN). This agrees well with the literature reviewed by Nanding et al. (2021), which highlights the role of the initial condition on the model sensitivity to relative rainfall errors. However, there are also important differences. The conditions that maximize the model sensitivity to rainfall errors are completely different for the two runoff-generation models analyzed here. First, whereas the PDM elasticity function shows a peak for normalized rainfall w_{pdm} equal to 1, at least for $b \leq 1$, the SCS-CN elasticity function monotonically decreases with increasing normalized rainfall. Hence, with the PDM module, the model sensitivity to rainfall errors tends to be large for values of precipitation close to the moisture capacity holding of the basin. Conversely, with the SCS-CN module, the model sensitivity to rainfall errors tends to be large for relatively small values of precipitation depth relative to the maximum potential retention.

Variations in the elasticity functions in the two models originate from two main differences between them: their initial conditions, and the lack of a store structure in the SCS-CN model. The structure of the initial abstractions with the SCS-CN module implies that no runoff may be generated even with a positive rainfall input. Analytically, this sets the conditions for an asymptotic tendency of the elasticity function to infinity when the normalized rainfall tends to zero. For the PDM, the soil moisture accounting structure of the model implies a proportionality relationship between direct runoff and rainfall, which translates into a unitary elasticity for infinitely small values of the normalized rainfall.

The occurrence of a peak in the elasticity function for the PDM is due to its soil moisture accounting (SMA) store structure. The SMA procedure is based on the notion that the higher the moisture store level, the higher the fraction of rainfall that is converted into runoff. When the store capacity is exhausted and all the rainfall is directly transformed into runoff, the elasticity should reach a maximum value (at least for $b \leq 1$), which corresponds to the peak. Wang (2018) presents a generalized probability density function for the variability of catchment soil moisture capacity that can describe both the SCS-CN and PDM models. Hence, we may expect that in this case the two models are characterized by the same elasticity function. It is interesting to note that this happens in Wang (2018) only when the initial abstraction is set to zero in the SCS-CN model and the parameter C_{max} is set to infinity in the PDM model, thus actually setting the conditions for the elasticity function being the same in the two models.

The comparison of the analytical elasticity functions with the elasticity values obtained by using discrete values of the rain errors shows that, although the analytical functions slightly differ from the values of elasticity for discrete values of precipitation of practical use (Fig. 10), nevertheless they provide robust indications on the peak of elasticity (for the PDM) and on the asymptotic behavior (for both models). The application to the Vaia flood event shows that the main assumptions of the approach leading to the elasticity functions are quite well met in this case. An important feature we have identified with the case study is also that, even though typical calibration procedures fail to provide sufficient information to discriminate hydrologic performance between model structures, remarkable differences arise in the propagation of rainfall errors in the two models. This should be considered when designing flood forecasting systems, for instance when multi-model ensembles for flood forecasting are developed (Ajani et al., 2006). The diverging characteristics of the models to rainfall error propagation, which can be examined in advance, should be considered for this purpose.

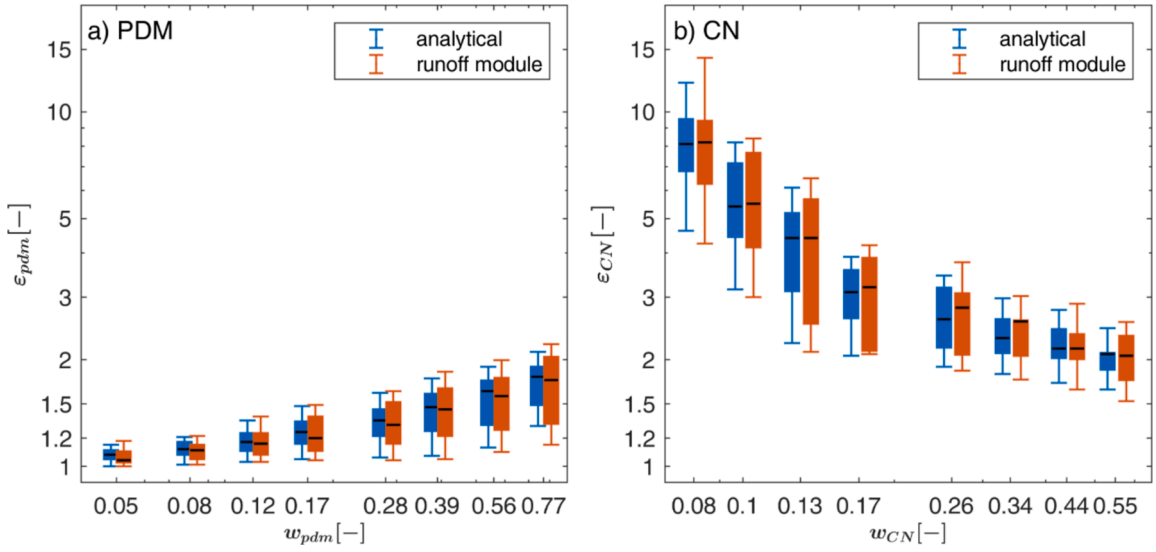

Fig. 10. Elasticity values obtained by using the analytically-derived elasticity functions and the runoff modules for various classes of normalized precipitation for a) PDM, and b) SCS-CN modules.

5. Conclusion

The objective of this work is to introduce the concept of the precipitation elasticity functions for hydrological models and to apply these functions for two well-known runoff generation model types: the Probability Distributed Model (PDM), where the Pareto distribution is used to describe the distribution of soil moisture storage capacity, and the SCS-CN model. The functions are exploited to analyze the propagation of rainfall errors through the two models.

It is shown that the two models are characterized by largely different elasticity functions, which results in contrasting propagation features of the relative rainfall errors. With the PDM, the elasticity function depends heavily on the parameter b, which describes the spatial variability of the storage capacity. For b less than 1, as considered in the case study of this work, elasticity starts at 1, then peaks at saturation, to retrace to 1 for large normalized precipitation approaching infinity. With the SCS-CN, elasticity decreases from infinity, at very low values of normalized precipitation, to 1 for large normalized precipitation approaching infinity. This shows that the two models transmit rainfall errors to runoff errors in a very different way. With the PDM, runoff errors tend to be small for low values of store filling, whereas with the SCS-CN model the errors tend to be very large in this case. In both cases, elasticity is larger for dry initial conditions.

An application to a major flood event in the Eastern Italian Alps, where the two hydrological models forced with input from a Numerical Weather Prediction (NWP) model were applied, provides an opportunity to examine in detail the main differences between the elasticity functions of the two models and their implications. It is shown that the analytical functions closely resemble the results obtained by forcing the models with the actual distribution of rainfall errors, thus providing robust indications on the peak of elasticity (for the PDM) and on the asymptotic behavior (for both models).

This study suggests that important benefits may accrue from considering the newly developed elasticity functions. Examining how different model structures propagate rainfall errors can be made in advance and should be considered when developing multi-model ensembles for more accurate flood forecasting systems. Analogously, the elasticity function could be considered for the development of new hydrological model calibration strategies, where novel objective functions capable of incorporating elasticity-based information on simulated discharge data could be tested.

Advancing our understanding of rainfall error propagation through hydrological models will potentially also aid in the investigation of the impacts of climate change (and associated uncertainty) on hydrological cycle components and water resource systems.

CRediT authorship contribution statement

E. Dallan: Writing – review & editing, Writing – original draft, Software, Methodology, Investigation, Conceptualization. **T. Perez-Ciria:** Writing – review & editing, Writing – original draft, Software, Methodology, Investigation. **L. Giovannini:** Writing – review & editing, Writing – original draft. **S. Davolio:** Writing – review & editing, Writing – original draft. **D. Zardi:** Writing – review & editing, Writing – original draft. **M. Borga:** Writing – review & editing, Writing – original draft, Methodology, Funding acquisition, Conceptualization.

Declaration of competing interest

The authors declare that they have no known competing financial interests or personal relationships that could have appeared to influence the work reported in this paper.

Acknowledgments

This study was carried out within the RETURN Extended Partnership and received funding from the European Union Next-GenerationEU (National Recovery and Resilience Plan—NRRP, Mission 4, Component 2, Investment 1.3—D.D. 1243 2/8/2022, PE0000005. This work was supported by CARIPARO Foundation, Italy, through the Excellence Grant 2021 to the “Resilience” Project. The Hydrographic Office of the Autonomous Province of Bolzano, Italy (http://meteo.provincia.bz.it) provided temperature, precipitation and streamflow data. This work was also performed as part of the IAHS HELPING Working Group on “ Hydrologic Design - Solutions & Communication".

Data availability

Data will be made available on request.

References

Anderson, B.J., Brunner, M.I., Slater, L.J., Dadson, S.J., 2024. Elasticity curves describe streamflow sensitivity to precipitation across the entire flow distribution. Hydrology and Earth System Sciences 28 (7), 1567–1583. https://doi.org/10.5194/hess-28-1567-2024, 2024.

Andreassian, V., Coron, L., Lerat, J., Le Moine, N., 2016. Climate elasticity of streamflow revisited—An elasticity index based on long-term hydrometeorological records. Hydrology and Earth System Sciences 20 (11), 4503–4524. https://doi.org/10.5194/hess-20-4503-2016.

Ajani, N.K., Duan, Q., Gao, X., Sorooshian, S., 2006. Multimodel Combination Techniques for Analysis of Hydrological Simulations: Application to Distributed Model Intercomparison Project Results. J. Hydrometeorol., 755–768. https://doi.org/10.1175/JHM519.1.

Beck, H.E., Vergopolan, N., Pan, M., Levizzani, V., van Dijk, A.I.J.M., Weedon, G.P., et al., 2017. Global-scale evaluation of 22 precipitation datasets using gauge observations and hydrological modeling. Hydrology and Earth System Sciences 21 (12), 6201–6217. https://doi.org/10.5194/hess-21-6201-2017.

Biemans, H., Hutjes, R., Kabat, P., Strengers, B., Gerten, D., Rost, S., 2009. Effects of precipitation uncertainty on discharge calculations for main river basins. J. Hydrometeor., 10, 1011–1025. https://doi.org/10.1175/2008JHM1067.1.

Dallan, E., Borga, M., Zaramella, M., Marra, F., 2022. Enhanced Summer Convection Explains Observed Trends in Extreme Subdaily Precipitation in the Eastern Italian Alps. Geophysical Research Letters 49(5), e2021GL096727. https://doi.org/10.1029/2021GL096727.

Dallan, E., Marra, F., M., Fosser, G., Marani, M., Formetta, G., Schär, C., and Borga M. 2023: How well does a convection-permitting regional climate model represent the reverse orographic effect of extreme hourly precipitation? Hydrol. Earth Syst. Sci., 27, 1133–1149, 2023 10.5194/hess-27-1133-2023.

Dallan, E., Borga, M., Fosser, G., Canale, A., Roghani, B., Marani, M., Marra, F., 2024a: A method to assess and explain changes in sub-daily precipitation return levels from convection-permitting simulations. Water Resources Research, 60, e2023WR035969. 10.1029/2023WR035969.

Dallan E., Marra F., Fosser G., Marani M., Borga M., 2024b: Dynamical factors heavily modulate the future increase of sub-daily extreme precipitation in the Alpine-Mediterranean region. Accepted in Earth’s Future.

Davolio, S., Malguzzi, P., Drofa, O., Mastrangelo, D., Buzzi, A., 2020. The Piedmont flood of November 1994: a test-bed of forecasting capabilities of the CNR-ISAC meteorological model suite. Bull. of Atmos. Sci. & Technol.,. https://doi.org/10.1007/s42865-020-00015-4.

Destro, E., Amponsah, W., Nikolopoulos, E., Marchi, L., Marra, F., Zoccatelli, D., Borga, M., 2018. Coupled prediction of flash flood response and debris flow occurrence: Application on an alpine extreme flood event. Journal of Hydrology 558, 225–237. https://doi.org/10.1016/j.jhydrol.2018.01.021.

Di Marco, N., Avesani, D., Righetti, M., Zaramella, M., Majone, B., Borga, M., 2021. Reducing hydrological modelling uncertainty by using MODIS snow cover data and a topography-based distribution function snowmelt model. J. Hydrol., 599, 126020. https://doi.org/10.1016/j.jhydrol.2021.126020.

Ehsan Bhuiyan, M.A., Nikolopoulos, E.I., Anagnostou, E.N., Polcher, J., Albergel, C., Dutra, E., Fink, G., Martínez-de la Torre, A., Munier, S., 2019. Assessment of precipitation error propagation in multi-model global water resource reanalysis. Hydrol. Earth Syst. Sci., 23, 1973–1994. https://doi.org/10.5194/hess-23-1973-2019.

Formetta, G., Dallan, E., M., Borga, M., Marra, F.,, 2024. Sub-daily precipitation returns levels in ungauged locations: Added value of combining observations with convection permitting simulations. Advances in Water Resources 194, 104851. https://doi.org/10.1016/j.advwatres.2024.104851.

Ghimire, G.R., Krajewski, W.F., Ayalew, T.B., Goska, R., 2022. Hydrologic investigations of radar-rainfall error propagation to rainfall-runoff model hydrographs. Advances in Water Resources 161, 104145. https://doi.org/10.1016/j.advwatres.2022.104145.

Giovannini, L., Davolio, S., Zaramella, M., Zardi, D., Borga, M., 2021. Multi-model convection-resolving simulations of the October 2018 Vaia storm over northeastern Italy. Atmospheric Res., 253, 105455. https://doi.org/10.1016/j.atmosres.2021.105455.

Gou, J., Miao, C., Sorooshian, S., Qingyun, D., Xiaoying, G., Ting, S., 2024. Satellite-based precipitation error propagation in the hydrological modeling chain across

China. Journal of Hydrology 632, 130906. https://doi.org/10.1016/j.jhydrol.2024.130906.
Gourley, J.J., Hong, Y., Flamig, Z.L., Wang, J., Vergara, H., Anagnostou, E.N., 2011. Hydrologic evaluation of rainfall estimates from radar, satellite, gauge, and combinations on Ft. Cobb basin. Oklahoma. J. Hydrometeor., 12, 973–988. https://doi.org/10.1175/2011JHM1287.1.
Hunt, A.G., Sahimi, M., Ghanbarian, B., 2023. Predicting streamflow elasticity based on percolation theory and ecological optimality. AGU. Advances 4, e2022AV000867. https://doi.org/10.1029/2022AV000867.
Koren, V.I., Finnerty, B.D., Schaake, J.C., Smith, M.B., Seo, D.J., Duan, Q.Y., 1999. 1999: Scale dependencies of hydrologic models to spatial variability of precipitation. J. Hydrol. 217, 285–302. https://doi.org/10.1016/S0022-1694(98)00231-5.
Liang, D.P., Lettenmaier, E.F., Wood, S.J., 1994. Burges, 1994: A simple hydrologically based model of land surface water and energy fluxes for general circulation models. J. Geophys. Res., 99 (D7), 14415–14428. https://doi.org/10.1029/94JD00483.
Loucks, D.P., van Beek, E., 2005. 2005: Water Resources Systems Planning and Management available from: UNESCO. France, Paris http://www.wldelft.nl/rnd/intro/fields/watermanagement/book.html (accessed 30.05.24.
Maggioni, V., Vergara, H.J., Anagnostou, E.N., Gourley, J.J., Hong, Y., Stampoulis, D., 2013. Investigating the applicability of error correction ensembles of satellite rainfall products in river flow simulations. J. Hydrometeor., 14, 1194–1211. https://doi.org/10.1175/JHM-D-12-074.1.
Markstrom, S.L., Hay, L.E., Clark, M.P., 2016. Towards simplification of hydrologic modeling: identification of dominant processes. Hydrol. Earth Syst. Sci. 20, 4655–4671. https://doi.org/10.5194/hess-20-4655-2016.
Mockus, V., 1972: National Engineering Handbook Section 4, Hydrology, NTIS, available at: https://directives.sc.egov.usda.gov/OpenNonWebContent.aspx?content=18393.wba (last access:19 December 2023).
Moore, R.J., 1985. The probability-distributed principle and runoff production at point and basin scales. Hydrol. Sci. J. 30, 273–297. https://doi.org/10.1080/02626668509490989.
Moore, R.J., 2007. The PDM rainfall-runoff model. Hydrol. Earth Syst. Sci. 11, 483–499. https://doi.org/10.5194/hess-11-483-2007.
Nanding, N., Wu, H., Tao, J., Maggioni, V., Beck, H., Zhou, N., Huang, M., Huang, Z., 2021. Assessment of Precipitation Error Propagation in Discharge Simulations over the Contiguous United States. J. Hydromet., 22 (8), 1987–2008. https://doi.org/10.1175/JHM-D-20-0213.1.
Nash, J. E., Sutcliffe, J. V., 1970: River flow forecasting through conceptual models. Part 1: A discussion of principles, J. Hydrol., 10, 282–290, 10.1016/0022-1694(70)90255-6, 1970.
Nijssen, B., Lettenmaier, D.P., 2004. Effect of precipitation sampling error on simulated hydrological fluxes and states: Anticipating the Global Precipitation Measurement satellites. Journal of Geophysical Research: Atmospheres 109. https://doi.org/10.1029/2003JD003497.
Nikolopoulos, E.I., Anagnostou, E.N., Borga, M., 2013. Using high-resolution satellite rainfall products to simulate a major flash flood event in northern Italy. Journal of Hydrometeorology 14, 171–185. https://doi.org/10.1175/JHM-D-12-09.1.
Nikolopoulos, E.I., Anagnostou, E.N., Hossain, F., Gebremichael, M., Borga, M., 2010. Understanding the Scale Relationships of Uncertainty Propagation of Satellite Rainfall through a Distributed Hydrologic Model. Journal of Hydrometeorology 11, 520–532. https://doi.org/10.1175/2009JHM1169.1.
Norbiato, D., Borga, M., Degli Esposti, S., Gaume, E. and Anquetin, S.: Flash flood warning based on rainfall thresholds and soil moisture conditions: An assessment for gauged and ungauged basins. Journal of Hydrology, 362(3–4), 274–290, doi: 10.1016/j.jhydrol.2008.08.023, 2008.
Norbiato, D., Borga, M., Merz, R., Blöschl, G., Carton, A., 2009. 2009: Controls on event runoff coefficients in the eastern Italian Alps. J. Hydrol., 375 (3–4), 312–325. https://doi.org/10.1016/j.jhydrol.2009.06.044.
Ponce, V.M., Hawkins, R.H., 1996. Runoff curve number: Has it reached maturity? J. Hydrol. Eng., 1 (1), 11–19. https://doi.org/10.1061/(ASCE)1084-0699(1996)1:1(11).
Schaake, J.S., 1990: From Climate to Flow. In Climate Change and US Water Resources; Waggoner, P.E., Ed.; John Wiley: New York, NY, USA, 1990; pp. 177–206. ISBN 9780471618386.
Scorpio and co-authors, 2022. Storm characteristics dictate sediment dynamics and geomorphic changes in mountain channels: A case study in the Italian Alps. Geomorphology 403, 108173. https://doi.org/10.1016/j.geomorph.2022.108173.
V.P. Singh D.K. Frevert . 950 pp., Water Resour. Publ., Highlands Ranch, Colo. Mathematical Models of Small Watershed Hydrology and Applications 2002.
Todini, E., 1996. The ARNO rainfall-runoff model. J. Hydrol., 175 (1–4), 339–382. https://doi.org/10.1016/S0022-1694(96)80016-3.
Wang, D., 2018. A new probability density function for spatial distribution of soil water storage capacity leads to the SCS Curve Number method. Hydrol. Earth Syst. Sci. 22, 6567–6578. https://doi.org/10.5194/hess-22-6567-2018.
Winchell, M., Gupta, H.V., and Sorooshian, S, 1998: On the effect of infiltration–saturation–excess runoff using radar-based rainfall estimates: Effects of algorithm uncertainty and pixel aggregation. Water Resour. Res. 1998 34 2655–2670 10.1029/98WR02009.
Wood, E.F., Lettenmaier, D.P., Zartarian, V.G., 1992. A land–surface hydrology parameterization with subgrid variability for general circulation models. J. Geophys. Res.-Atmos., 97, 2717–2728. https://doi.org/10.1029/91JD01786.
Zhao, R.J., 1992. The Xinanjiang model applied in China. J Hydrol 135 (1–4), 371–381. https://doi.org/10.1016/0022-1694(92)90096-E.
Zhu., D., Peng, Z., and I. D. Cluckie, 2013: Statistical analysis of error propagation from radar rainfall to hydrological models. Hydrol. Earth Syst. Sci., 17, 1445–1453, www.hydrol-earth-syst-sci.net/17/1445/2013/doi:10.5194/hess-17-1445-2013.
Zoccatelli, D., Borga, M., Viglione, A., Chirico, G.B., Blöschl, G., 2011. 2011: Spatial moments of catchment rainfall: rainfall spatial organisation, basin morphology, and flood response. Hydrol. Earth Syst. Sci., 15, 3767–3783. https://doi.org/10.5194/hess-15-3767-2011.